Supporting Information

Bottlebrush Copolymer Additives for Immiscible Polymer Blends

Adeline Huizhen Mah, [†‡] Pantea Afzali,[‡] Luqing Qi,[§] Stacy Pesek,[§] Rafael Verduzco,[§]* Gila E. Stein[#]*

[†] Materials Science and Engineering Program, University of Houston, Houston TX 77204;

[‡]Department of Chemical and Biomolecular Engineering, University of Houston, Houston TX 77204;

[§] Department of Chemical and Biomolecular Engineering, Rice University, Houston TX 77006;

Department of Chemical and Biomolecular Engineering, University of Tennessee, Knoxville TN 37996

* gstein4@utk.edu, rafaelv@rice.edu

I. Materials

Random Copolymer Macromonomer. Linear poly (styrene-r-methyl methacrylate) macromonomers, NB-(P(S-r-MMA))-CTA, were synthesized via RAFT polymerization. S, MMA, NB-CTA (100mg, 0.18mmol) and AIBN (2.95mg, 0.018) mmol were added into a 10mL round bottom flask. The solution was purged with nitrogen gas for 30 minutes. The polymerization was initiated by placing the flask in an oil bath at 65°C. After 6 hours, the flask was removed and quenched by immersing in an ice bath. The polymer was then obtained by precipitating in methanol at 4°C and dried under vacuum. Table S1 lists the respective feed ratios of Styrene: MMA to generate the desired styrene compositions in the random copolymer macromonomer.

Target Styrene Mol Ratio in Macromonomer	Feed Mol Ratio	
	Styrene	MMA
0.6	0.5	0.5
0.5	0.3	0.7
0.4	0.1	0.9

Table S1: Feed ratios of Styrene and MMA for targeted styrene compositions in random copolymer macromonomers

Diblock Copolymer. PMMA-b-PS was prepared via two reversible addition–fragmentation chain transfer (RAFT) polymerizations. First, we prepare the PMMA macro-CTA by mixing MMA (1.82 g, 18.13 mmol), CTA (172.92 mg, 0.474 mmol), AIBN (7.84mg, 4.77×10^{-2} mmol) and benzene (anhydrous, 6mL) in a 25 mL round bottom flask, and the solution was purged with nitrogen gas for 30mins. by placing the flask in an oil bath at 65°C. After 12 hours, the flask was removed and quenched by immersing in an ice bath. The polymer was then obtained by precipitating in methanol at 4°C and dried under vacuum.

Next, we mixed the PMMA Macro-CTA dry product (529mg, 9.63×10^{-2} mmol), styrene (1.49g, 14.33 mmol), AIBN (14.66 mg, 8.93×10^{-2} mmol) and benzene (anhydrous, 2mL) in a 10 mL round bottom flask, and the solution was purged with nitrogen gas for 30mins. by placing the flask in an oil bath at 60°C. After 22 hours, the flask was removed and quenched by immersing in an ice bath. The polymer was then obtained by precipitating in methanol at 4°C and dried under vacuum. The M_n was 11860g/mol with a DP of 111(DP_{PMMA}=50 and DP_{PS}=61) and Đ=1.45. The PS content of the diblock was 56%

Gel Permeation Chromatography (GPC)

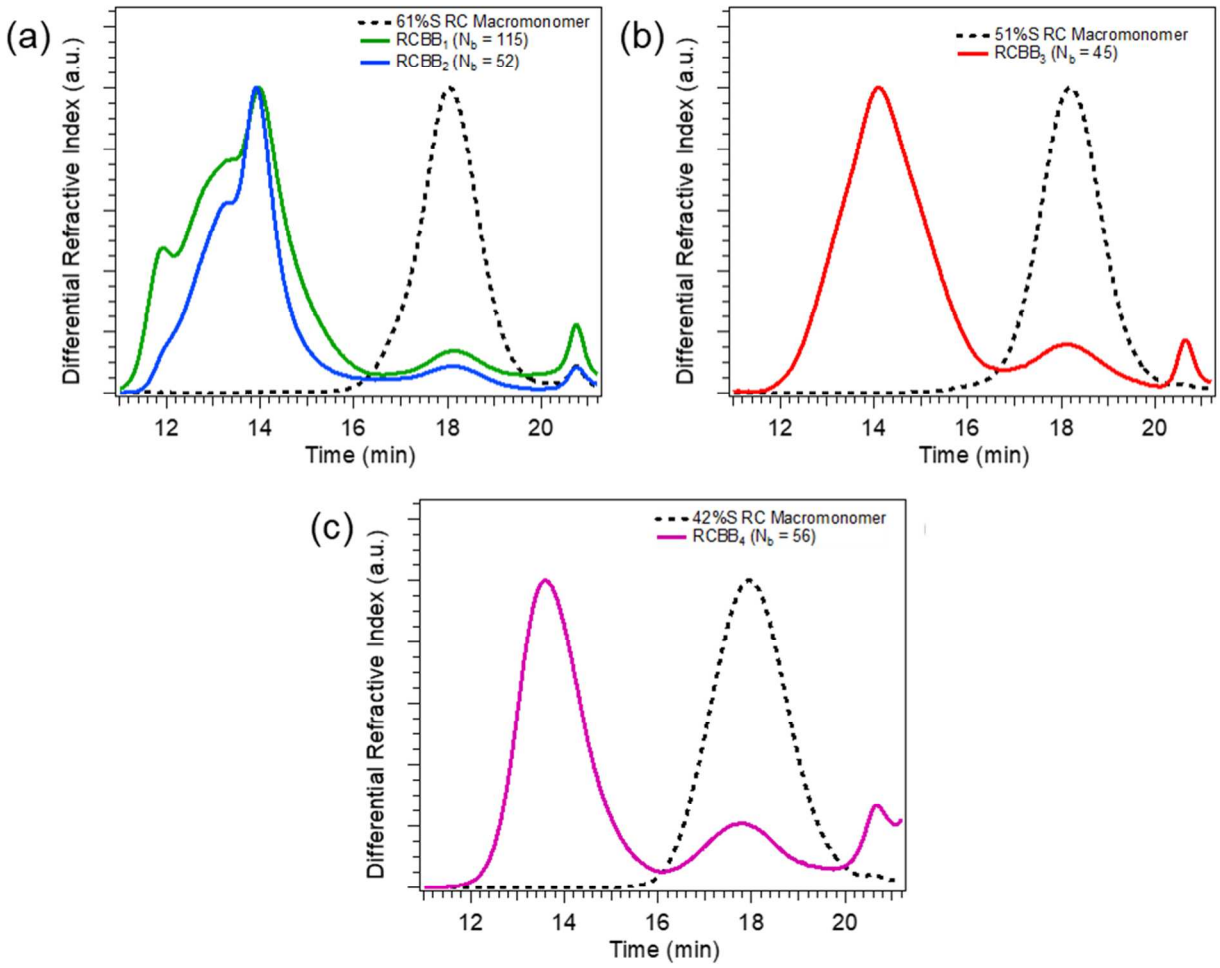

Figure S1: Size-exclusion chromatography analysis of RC bottlebrush polymers and macromonomers. (a) 61% styrene system consisting of $RCBB_1$ (N_b = 115) and $RCBB_2$ (N_b = 52). Each is 92% bottlebrush and 8% macromonomer. $RCBB_1$ has three molecular weight modes centered at 243, 501 and 2070 kg/mol. With integration of the peaks from the RI signal, and assuming the same dn/dc values for each peak, we estimate that the weight fractions of each mode are 0.58, 0.32, and 0.10, respectively. $RCBB_2$ has three molecular weight modes centered at 234, 445 and 1800 kg/mol, with approximate weight fractions of 0.62, 0.34, and 0.04, respectively. (b) 51% styrene system with $RCBB_3$ (N_b = 45), 89% bottlebrush and 11% macromonomer; (c) 42% styrene system with $RCBB_4$ (N_b = 56), 82% bottlebrush and 18% macromonomer.

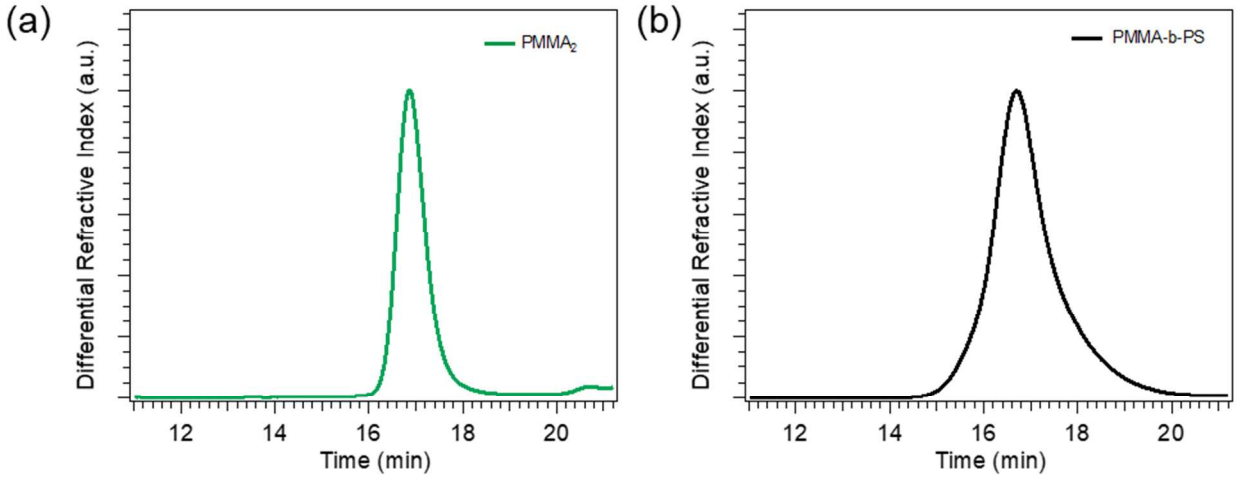

Figure S2: Size-exclusion chromatography analysis of (a) linear $PMMA_2$ and (b) diblock PMMA-b-PS.

Nuclear Magnetic Resonance (NMR) Spectra

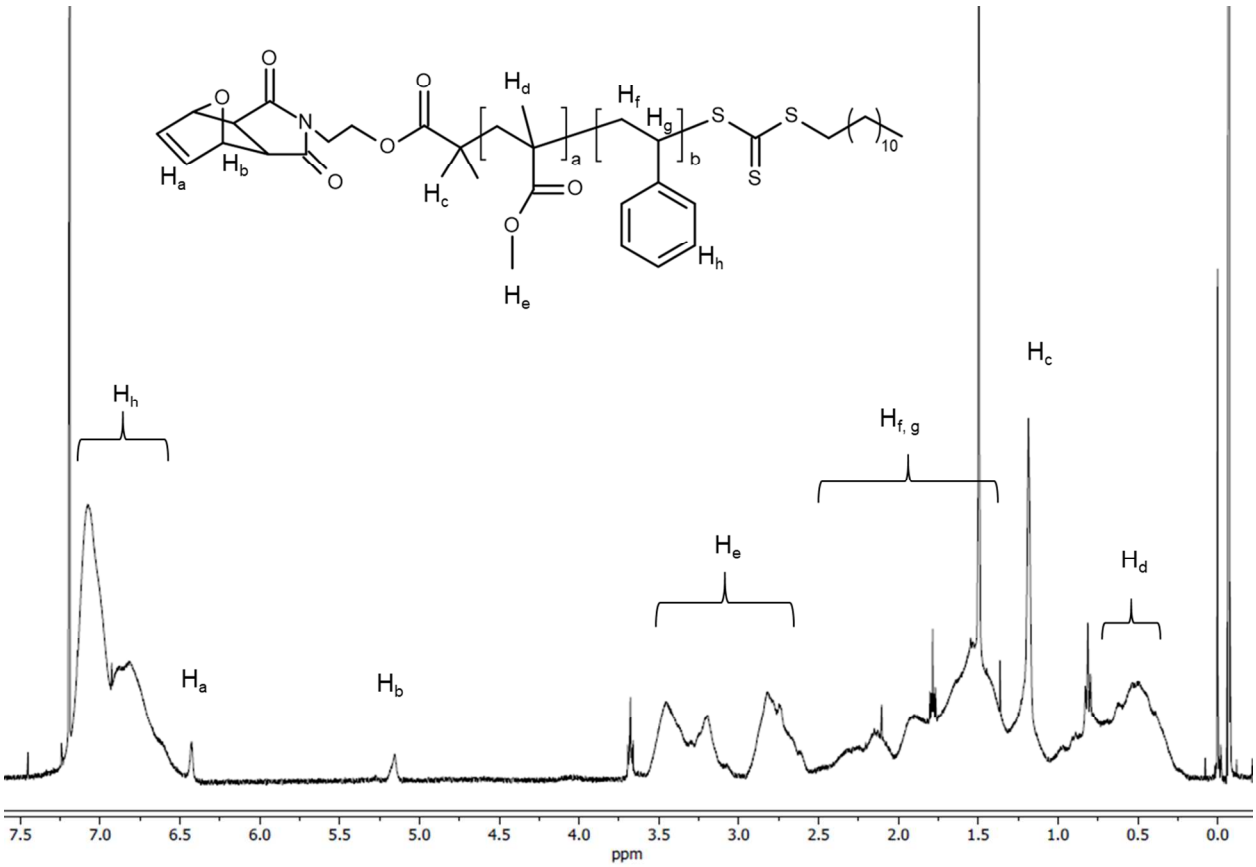

Figure S3: ^{1}H NMR spectrum for random copolymer macromonomer, 61%S NB-P(S-r-MMA)-CTA.

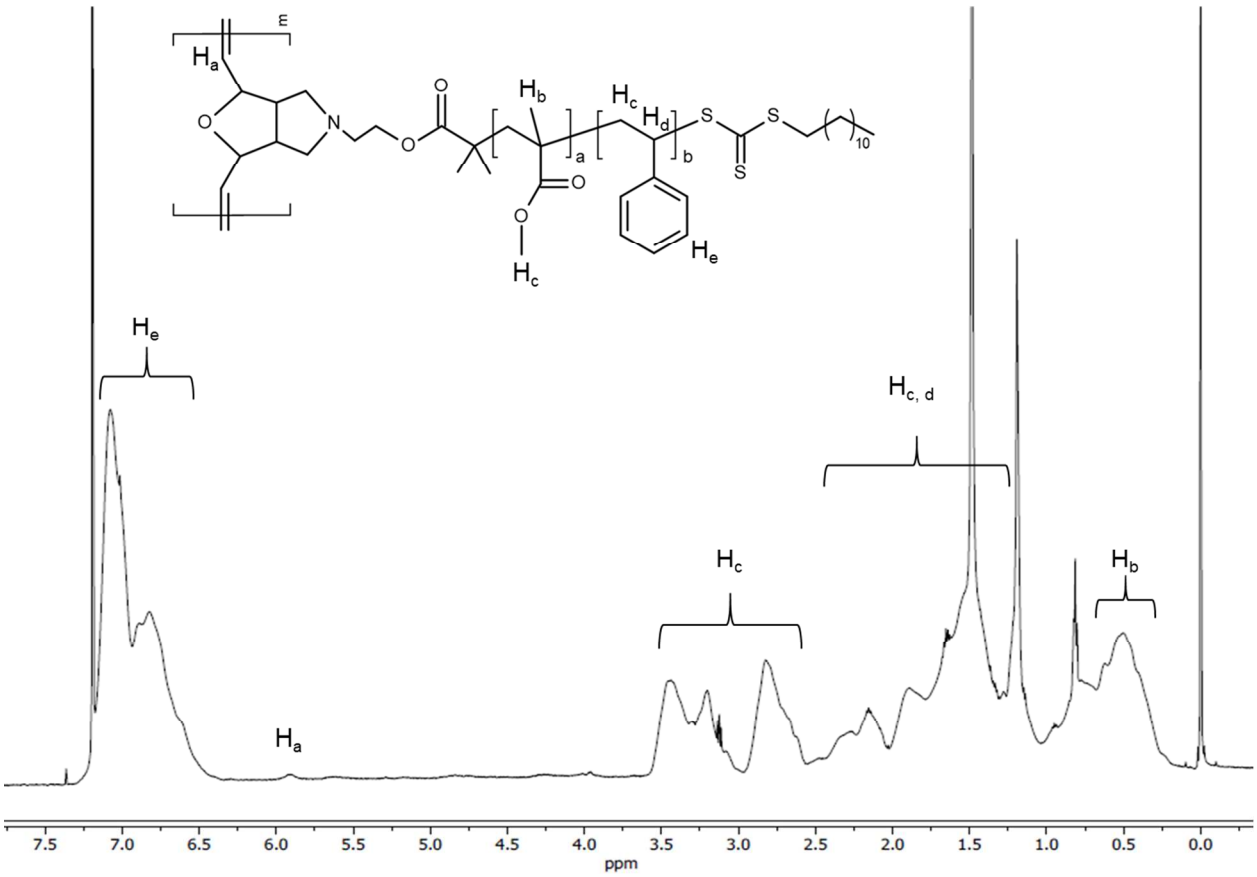

Figure S4: ^{1}H NMR spectrum for random copolymer bottlebrush polymer, P(NB-P(S-r-MMA)-CTA), $RCBB_1$

II. Thermal Stability (in Air)

The thermal stability of PS and PMMA (in air) has been extensively studied through thermal gravimetric analysis and Fourier-transform infrared (FTIR) spectroscopy,[5–8] and degradation is not detected over the course of hours at moderate annealing temperatures. To confirm this holds for the present materials, we performed FTIR measurements of PS_1, $PMMA_3$, and $RCBB_3$ films as a function of time at 150 ˚C. The results are summarized in the following figures. PS_1 and $RCBB_3$ samples were drop-cast onto silicon from toluene, while $PMMA_3$ was drop-cast from a toluene/acetone mixture. Films were annealed on a hotplate in air, then quenched to room temperature and measured in attenuated total reflectance mode. A baseline was subtracted using a "point-and-click" Matlab routine, meaning a user-defined baseline, and the same points (wavenumbers) were selected within each data set. Each measurement is from a different area on the sample, which leads to some noise, but there is no systematic trend as a function of time. Data are arbitrarily scaled to superimpose; if degradation occurs, then superposition would fail.

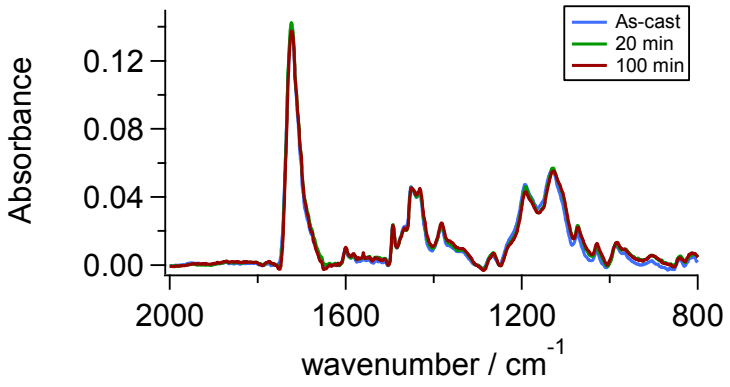

Figure S5: $RCBB_3$, wavenumbers 2000 to 800 cm^{-1}.

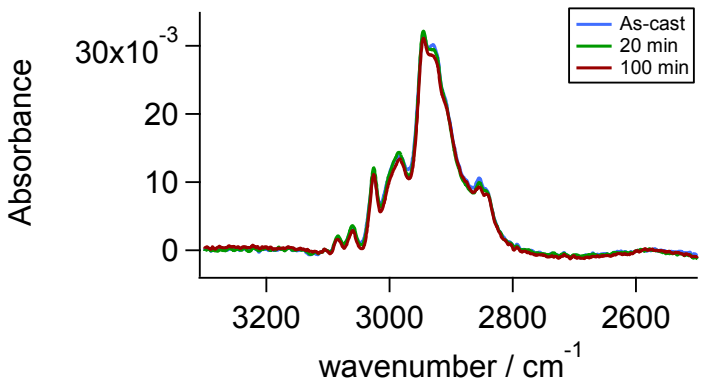

Figure S6: $RCBB_3$, wavenumbers 3300 to 2500 cm^{-1}.

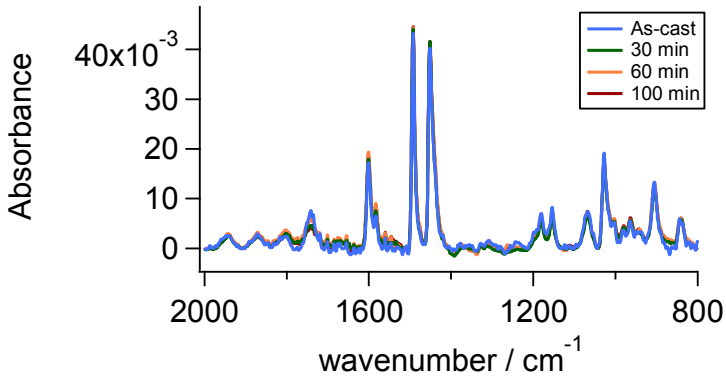

Figure S7: PS_1, wavenumbers 2000 to 800 cm^{-1}.

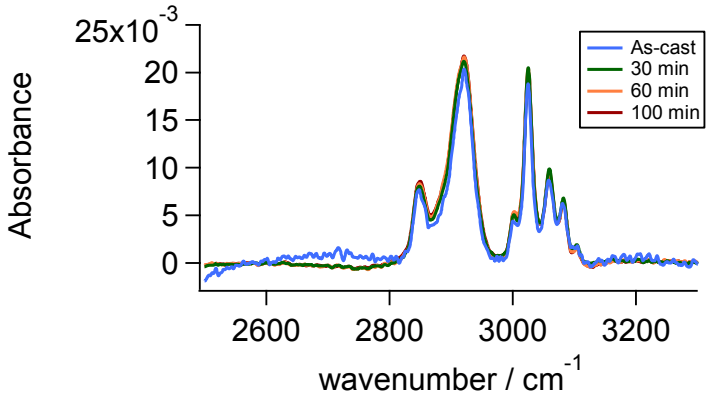

Figure 8: PS_1, wavenumbers 3300 to 2500 cm^{-1}.

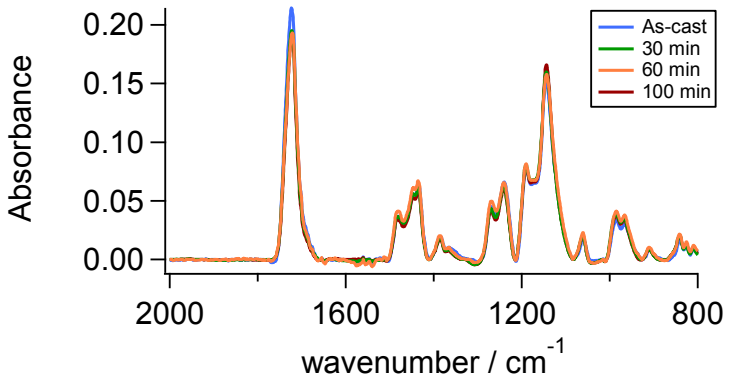

Figure S9: $PMMA_3$, wavenumbers 2000 to 800 cm^{-1}. The as-cast data have a stronger carbonyl signal at 1720 cm^{-1} due to residual acetone. Note that the peaks are invariant with time from 30 to 100 min.

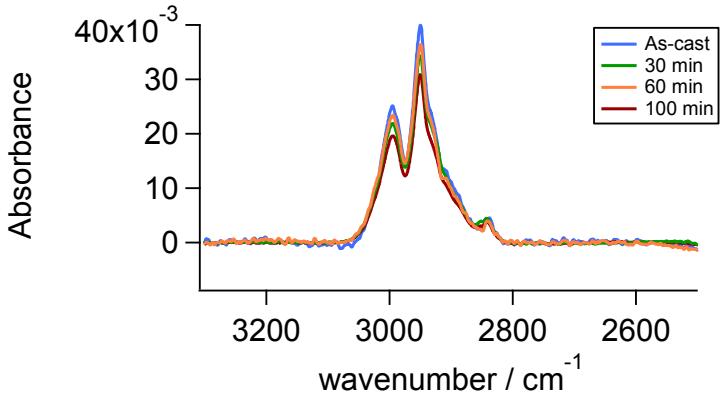

Figure S10: $PMMA_3$, wavenumbers 3300 to 2500 cm^{-1}. Acetone also absorbs near 3000 cm^{-1}.

III. Instrumentation

Optical Microscopy. Bright-field optical micrographs at 50x and 100x magnification were obtained using a Nikon LV100 light reflective microscope. These data reveal variations in film thickness across a sample.

IV. Analysis

Determination of Mw of Bottlebrush and PMMA Linear Polymers. As mentioned before, the molecular weights and polydispersities of the RCBB polymers were determined using GPC. First, we prepare known concentrations of RCBB polymer solutions from THF. Second, we determine the conversion of MM to RCBB. Next, we calculate the differential refractive index increment, dn/dc of the bottlebrush polymers in THF using a built-in script in the ASTRA program. The dn/dc value obtained is based on a 100% mass recovery assumption. However, this assumption will not be accurate since every bottlebrush sample contains a small amount of unreacted macromonomers. The dn/dc values are then corrected to reflect the conversion of MM to RCBB. This is done by dividing the initial dn/dc values obtained with the corresponding RCBB conversion values obtained at the beginning. The corrected dn/dc values are specified for the RCBB peaks and the data from the light scattering measurements are fitted using the Zimm model to obtain the molar mass of these RCBB polymers. The Mw of these RCBB polymers are then calculated from the molar mass obtained. In addition, we determine the polydispersities of the RCBB polymers from the conventional calibration method with a polystyrene column. In the case of PMMA linear polymers, we employ the same method we used for the bottlebrush polymers but without corrections to the dn/dc values.

V. Supplemental Data

Flory-Huggins

We used the Flory-Huggins model to estimate the following parameters for neat blends (no additive):

1) The composition of PS in PS-rich and PMMA-rich phases, i.e., φ_{PS}^{α} and φ_{PS}^{β};
2) The critical composition of each blend, $\Phi_{C,PS}$; and
3) The overall blend composition where the majority and minority phases invert, $\Phi_{I,PS}$.

The outcomes are summarized in Table S2 below. We assume a monomer volume of 0.179 nm^3 for PS, 0.149 nm^3 for PMMA, and $\chi = 0.018$ at 150 °C for a reference volume of 0.1 nm^3. All of these parameters were taken from the review by Eitouni and Balsara that is referenced in the manuscript [3]. The methods for calculating equilibrium compositions and critical compositions are described in the same reference. The composition that marks phase inversion is estimated from a mass balance using $V^{\alpha} = V^{\beta} = 0.5$:

(1) $\Phi_{PS} = \varphi_{PS}^{\alpha} V^{\alpha} + \varphi_{PS}^{\beta} V^{\beta} = \left(\varphi_{PS}^{\alpha} + \varphi_{PS}^{\beta}\right)/2$

Table S2: Predicted thermodynamic properties of neat blends.

Blend	φ_{PS}^{α}	φ_{PS}^{β}	$\Phi_{C,PS}$	$\Phi_{I,PS}$
PS1/PMMA1	0.97	0.01	0.49	0.49
PS1/PMMA2	0.97	0.02	0.47	0.49
PS2/PMMA3	0.99	2e-03	0.40	0.49

As-Cast Data for PS/PMMA Blend Films

Figure S11 shows the as-cast films of PS_1:$PMMA_1$ blends at volume ratios 57:43 with (a) no additive and (b) 20 vol% $RCBB_1$ additive. These films exhibited bumps at the surface and are approximately 0.5 µm in diameter and 80 nm tall.

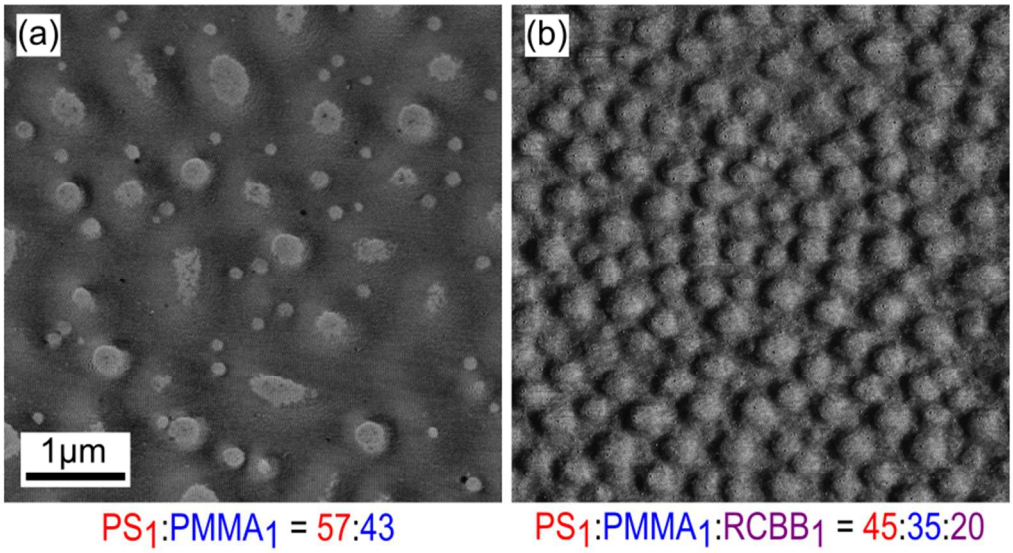

Figure S11: AFM phase images of as-cast PS_1:$PMMA_1$ blends at 57: 43 proportions. (a) No additive and (b) 20 vol% RCBB Blends.

Selective Removal of PS Phase

To test for the uniformity of the microstructures formed throughout the film thickness, we selectively removed the PS phase using cyclohexane. This test is performed by soaking the samples in cyclohexane for at least 60 seconds and was dried with nitrogen gas. We performed this test on two blend systems i.e. the low molecular weight PS_1 and $PMMA_1$ and the high molecular weight PS_2 and $PMMA_3$

Figure S12 shows the before and after cyclohexane treatment on a 46:54 PS_1: $PMMA_1$ with 20 vol% $RCBB_1$ additive sample that is annealed for 85 minutes. From the optical

microscopy image of the pretreated sample (Figure S12a), we observe a relatively smooth surface with a slight thickness variation over short length scales. In the AFM phase image (Figure S12b), we observe individual PMMA domains encapsulated by a RCBB-rich "shell" in a PS-rich majority phase. Further image analysis on the AFM phase image indicates that the combined fractional area of PMMA and $RCBB_1$ is 0.50, or 50 vol%. After the cyclohexane treatment, we observe clear individual microstructures in the optical microscopy image (Figure S12c) indicating that the PS phase was uniformly removed throughout the film thickness. This is confirmed through the AFM height image (Figure S6d) which shows the remaining microstructures, i.e., PMMA domains with the RCBB encapsulation. Further analysis shows that the combined fractional area of PMMA and RCBB is 0.53, or 53 vol%. This shows that the content of PMMA and RCBB are very similar with a slight 3 vol% increase. We then analyze the roughness profile (Figure S13) of the cyclohexane treated sample and saw that the height of the microstructures was uniform throughout the film thickness.

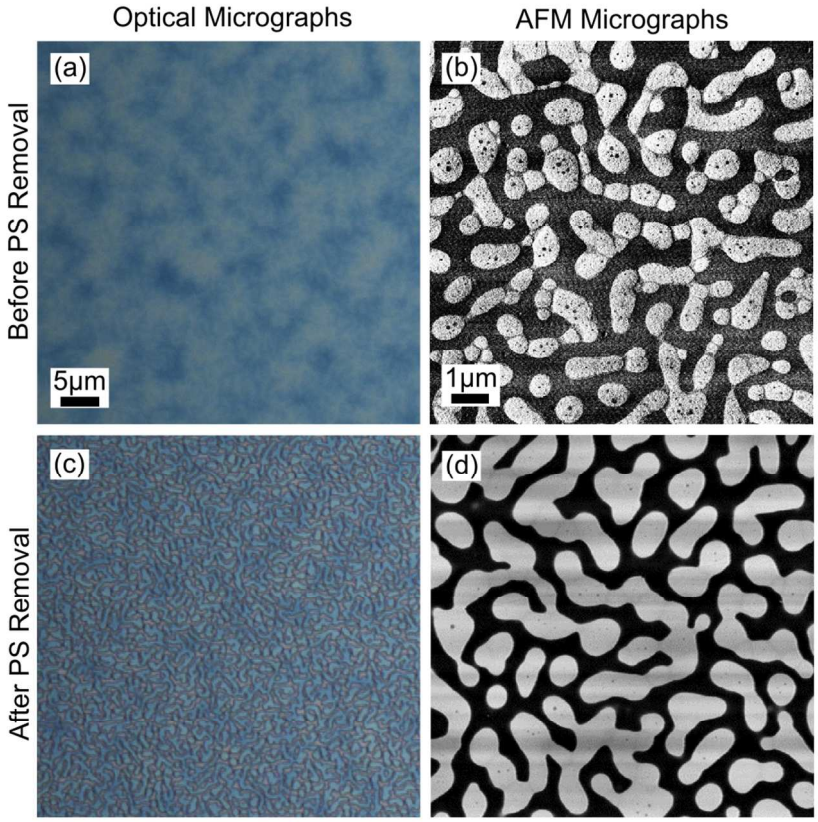

Figure S12: OM and AFM Images for before PS phase removal (a-b) and after PS phase removal (c-d) for 43:57 PS_1:$PMMA_1$ blend with 20 vol% $RCBB_1$ additive.

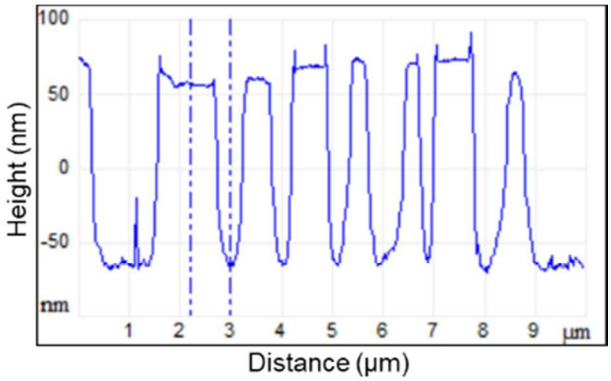

Figure S13: AFM Roughness Profile for 43:57 PS_1:$PMMA_1$ blend with 20 vol% $RCBB_1$ additive after PS phase removal.

Figure S14 shows the before and after cyclohexane treatment on a 57:43 PS_2: $PMMA_3$ blend with 20 vol% of $RCBB_1$ additive that is annealed for 85 minutes. From the optical microscopy image of the pretreated sample (Figure S14a), we observe a rough surface with significant thickness variations over short length scales. Upon further inspection of the AFM phase image (Figure S14b) we observe the same rough profile observed in Figure S7a with a PS-rich majority phase and individual PMMA domains that are encapsulated by a RCBB phase. The combined relative volume of PMMA and RCBB was determined to be 25%. After the cyclohexane treatment, we do not observe clear individual microstructures in the optical microscopy image (Figure S14c) which indicates that the microstructures are not uniform throughout the film. The AFM height micrograph (Figure S8d) shows a larger distribution of the microstructures consisting of PMMA and RCBB with a 34 vol%, i.e., a 14 vol% increase. Analysis of the roughness profile (Figure S15) shows that the microstructures are not uniform throughout the film, which is also seen through observation of the optical microscopy images (Figure S14c).

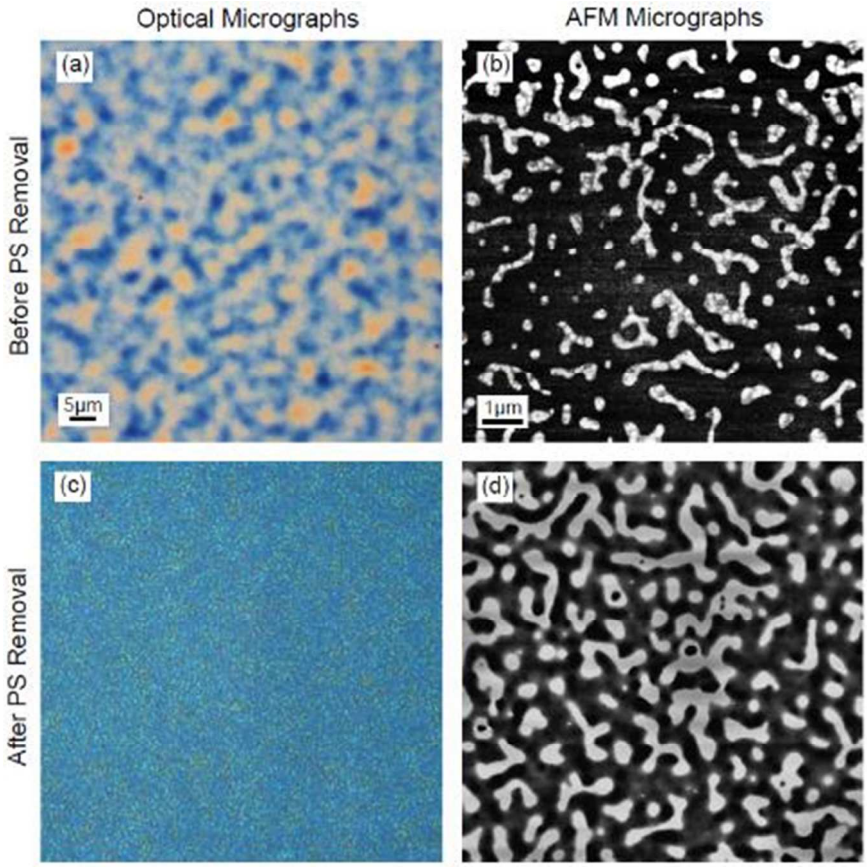

Figure S14: OM and AFM Images for before PS phase removal (a-b) and after PS phase removal (c-d) for 57:43 PS_2:$PMMA_3$ blend with 20 vol% of $RCBB_1$ additive.

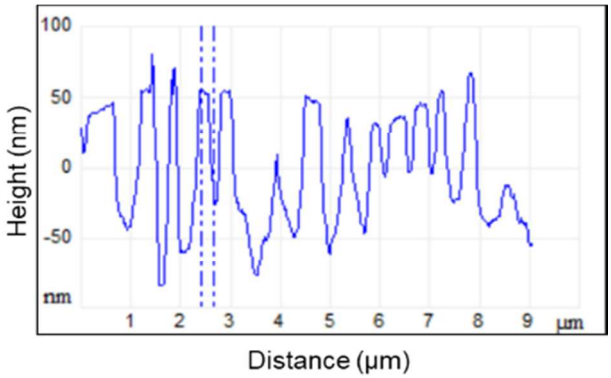

Figure S15: AFM Roughness Profile for 57:43 PS_2:$PMMA_3$ blend with 20 vol% $RCBB_1$ additive after PS phase removal.

Domain Size Distribution of $PS_1/PMMA_1$ Blends with No Additive and RC

Figure S16 illustrates the time evolution of the minority domain size distribution for PS_1:$PMMA_1$ blend volume ratios of 57:43 and 47:53 with no additive (Figure S16(a-b)) and with 20 vol% RC (Figure S16(c-d)). These plots show that the minority domains (PS or PMMA, depending on the blend composition) coarsen with time in all cases except for the 57:43 PS_1: $PMMA_1$ blend with 20 vol% RC.

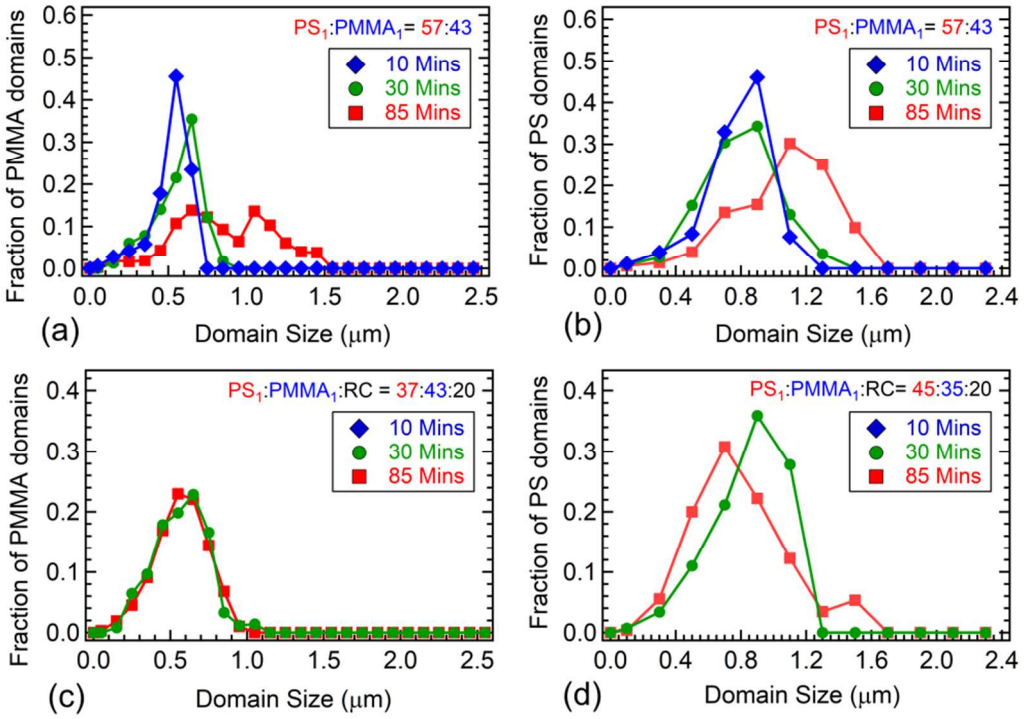

Figure S16: Domain size distribution of $PS_1/PMMA_1$ blends with (a,b) no additive and (c,d) 20 vol% RC. Relative volume of $PS_1/PMMA_1$ blend constituents is fixed in each column (left: 57:43, right: 46:54).

Side Chain Composition Effects

Table S3: Properties of RCBB additives. RCBB side chains have composition f_{PS} (mole fraction styrene), degree of polymerization N_{sc}, and dispersity $Đ_{sc}$. Backbone degree of polymerization and dispersity are N_b and $Đ_b$, respectively.

Tag	f_{PS}	N_{sc}	$Đ_{sc}$	N_b	$Đ_b$
$RCBB_2$	0.61	59	1.20	52	1.4
$RCBB_3$	0.51	57	1.27	45	1.6
$RCBB_4$	0.42	57	1.36	56	1.4

We studied the effects of composition on phase behavior by preparing bottlebrush additives with side chains containing styrene molar ratios, f_s of 0.61 ($RCBB_2$), 0.51 ($RCBB_3$) and 0.42 ($RCBB_4$). These bottlebrush additives have similar backbone and side chain lengths. Next, we prepared ternary blends with PS_1:$PMMA_2$ volume ratios of 57:43, 52:48 and 47:53 with 20 vol% bottlebrush additives of each composition. As stated earlier, we expect a phase inversion from a majority PS-rich phase to a majority PMMA-rich phase at $\Phi_{,PS} \approx 0.5$.

Figure S17 reports the AFM phase image of the ternary blends with the respective bottlebrush additive. At a fixed blend volume ratio of 57:43 PS_1:$PMMA_2$ with 20 vol% $RCBB_i$ Additive (PS_1/$PMMA_2$/$RCBB_i$ = 45:35:20) (Figures S17a-c), we expect the blend to phase-separate into a PS-rich matrix with PMMA-rich minority domains. This behavior is observed when f_s=0.61, and the PS phase appears to be swollen as discussed in the manuscript. (We do not perform mass balances on these data, as the structures are not uniform with depth into the film.) However, when f_s=0.51, the blend phase separates into a co-continuous structure where the sizes of PS-rich and PMMA-rich channels are approximately the same. When f_s= 0.42, the blend phase separates into a PMMA-rich matrix with PS-rich minority domains.

At a fixed blend volume ratio of 52:48 PS_1:$PMMA_2$ with 20 vol% $RCBB_i$ additive (PS_1/$PMMA_2$/$RCBB_i$ = 42:38:20) (Figures S17d-f), we expect the blend to phase-separate into co-continuous PS-rich and PMMA-rich domains. We observe this behavior when f_s=0.51. When f_s=0.61, the blend phase separates into a PS-matrix and PMMA-rich minority domains. When f_s= 0.42, the blend phase separates into a PMMA-rich matrix with PS-rich minority domains.

In addition, at a fixed blend volume ratio of 47:53 PS_1:$PMMA_2$ with 20 vol% $RCBB_i$ Additive (PS_1/$PMMA_2$/$RCBB_i$ = 37:43:20) (Figures S17g-i), we expect the blend to phase-separate into majority PMMA-rich matrix with PS-rich minority domains. We observe this behavior when f_s=0.51 and 0.42. However, when f_s=0.61, the blend phase separates into a co-continuous structure of approximately equal PS and PMMA channels. The trends at all blend compositions clearly show that bottlebrush composition can be tuned to control the miscibility in each phase, which in turn controls the blend microstructure.

These changes in morphology are due to the relationship between the chemical composition of the side chains and homopolymers. By tuning the chemical compositions of the side chains, we modify its compatibility in the PS and PMMA homopolymers. For example, at a fixed blend composition of 52:48 PS_1: $PMMA_2$, we observe the area of PS-rich domains increases with increasing styrene content in the side chains. We attribute this behavior to the increase in contact of the styrene monomers from both the homopolymer and side chains which enhances its distribution in the PS homopolymer matrix[2]. These data suggest the "optimal" composition for equal solubility in PS and PMMA is closer to 50% styrene than 60% styrene.

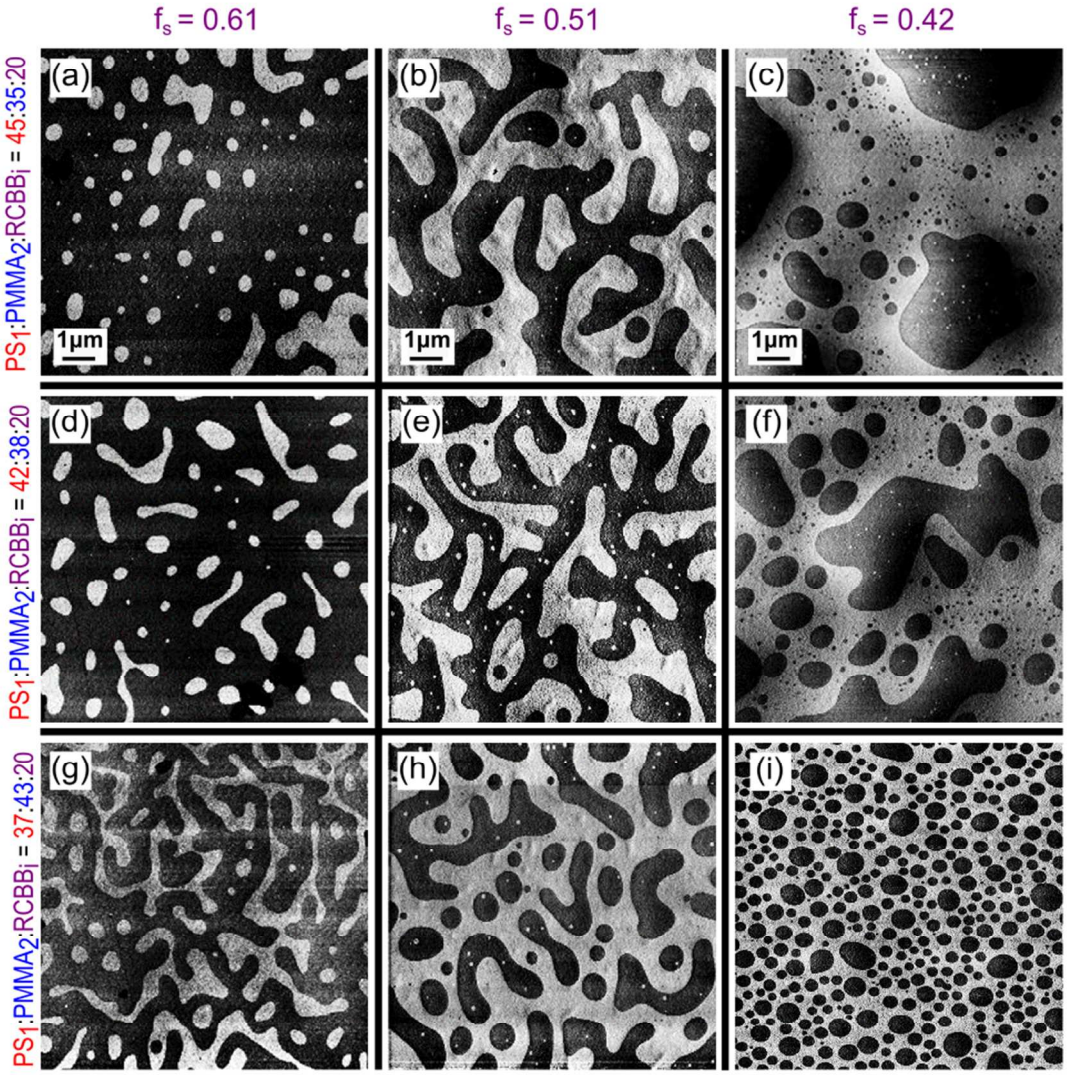

Figure S17: AFM phase images of PS_1/$PMMA_2$ blends with 20 vol% RCBB additives at different side chain composition and blend volume ratios (a-c) 57:43, (d-f) 52:48 and (g-i) 47:53.

Optical Microscopy Data for PS_1 and $PMMA_1$ Blends with 20vol% $RCBB_1$

Figure S18 shows the optical microscopy images for PS_1:$PMMA_1$ blend volume ratios of 57:43 (Figure S18a) and 47:53 (Figure S18b) with 20 vol% of $RCBB_1$ additive. These images show some thickness variation over a 5µm length scale. The height of these thickness variations is approximately 50 nm based on color variation.

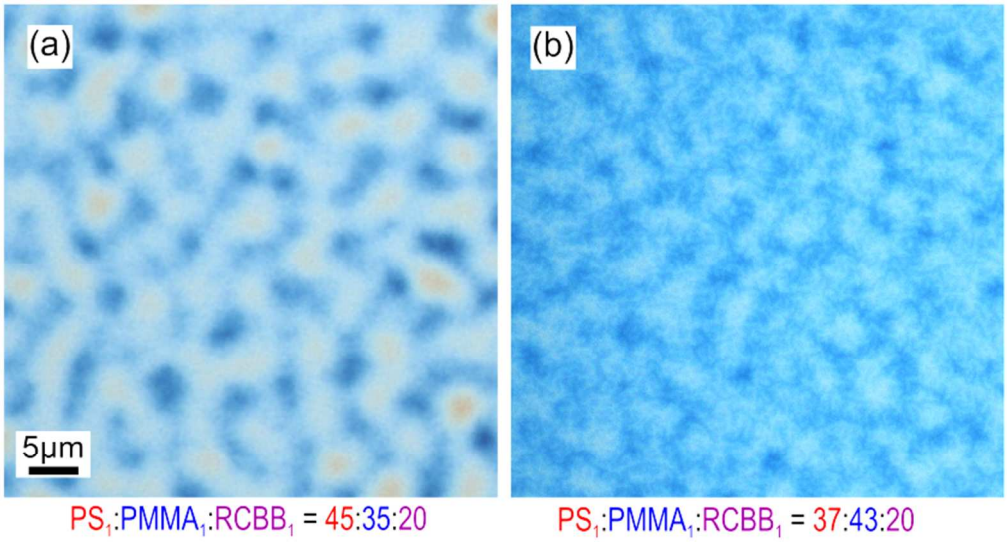

Figure S18: OM images of PS_1/$PMMA_1$ blends with 20 vol% $RCBB_1$ annealed for 85 minutes. Relative volume of PS_1/$PMMA_1$ blends is fixed at (a) 57:43 and (b) 47:53.

Optical Microscopy and AFM Data for PS_1 and $PMMA_2$ Blends with 20 vol% $RCBB_1$

Figure S19 reports the AFM phase images for the 57:43 PS_1:$PMMA_2$ blend with 20 vol% of $RCBB_1$ additive as a function of time. Further quantitative analysis on the AFM micrographs (Figure S20) indicates that the PMMA domains coarsen with time.

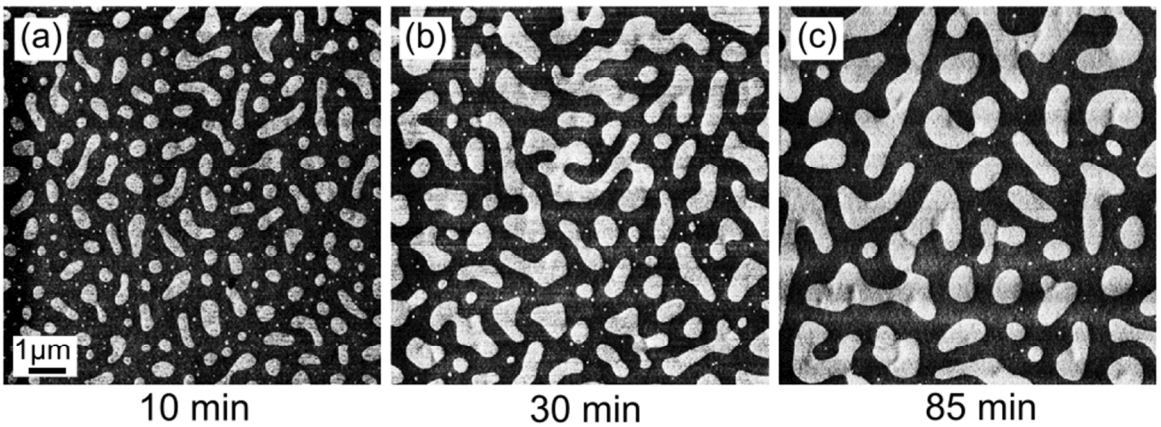

Figure S19: AFM phase images of 57:43 PS_1/$PMMA_2$ blends with 20 vol% of RCBB additive. (a) 10 min; (b) 30 min; and (c) 85 min.

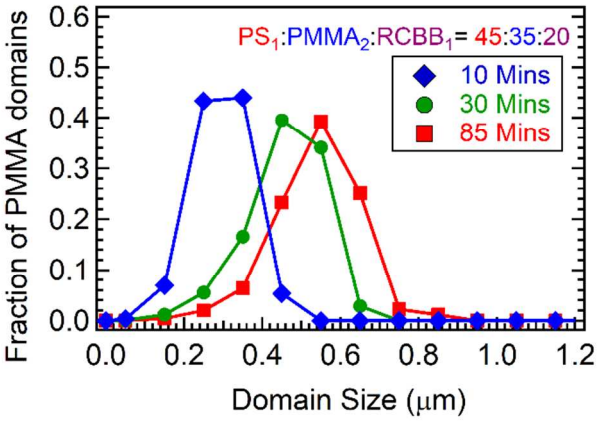

Figure S20: Domain size distribution of 57:43 PS_1/$PMMA_2$ blends with 20 vol% of $RCBB_1$ additive.

The optical microscopy images for PS_1:$PMMA_2$ blends vol ratios 57:43, 52:48 and 43:57 with 20 vol% of $RCBB_1$ additive after 85 minutes of annealing are reported in Figure S21. These images show that there are slight thickness variations over a 5µm length scale.

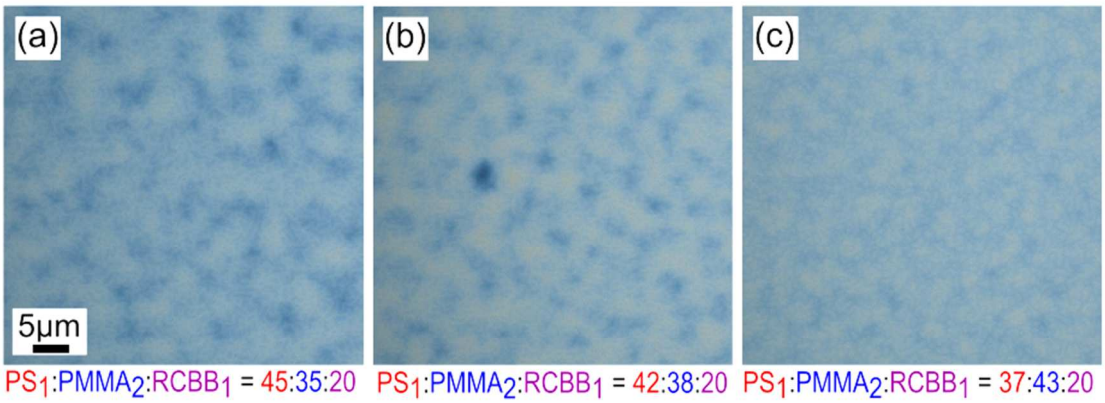

Figure S21: OM images of PS_1/$PMMA_2$ blends with 20 vol% $RCBB_1$ annealed for 85 minutes. Relative volume of PS_1/$PMMA_2$ blends is fixed at (a) 57:43, (b) 52:48 and (c) 47:53.

Optical Microscopy and AFM Data for PS_2 and $PMMA_3$ Blends with 20 vol% $RCBB_1$

Figure S22 reports the AFM phase images for the 57:43 PS_2:$PMMA_3$ blend with 20 vol% $RCBB_1$ additive as a function of time. Further qualitative analysis on the AFM micrographs (Figure S23) indicate that the coarsening of the PMMA domains is arrested at 30 mins.

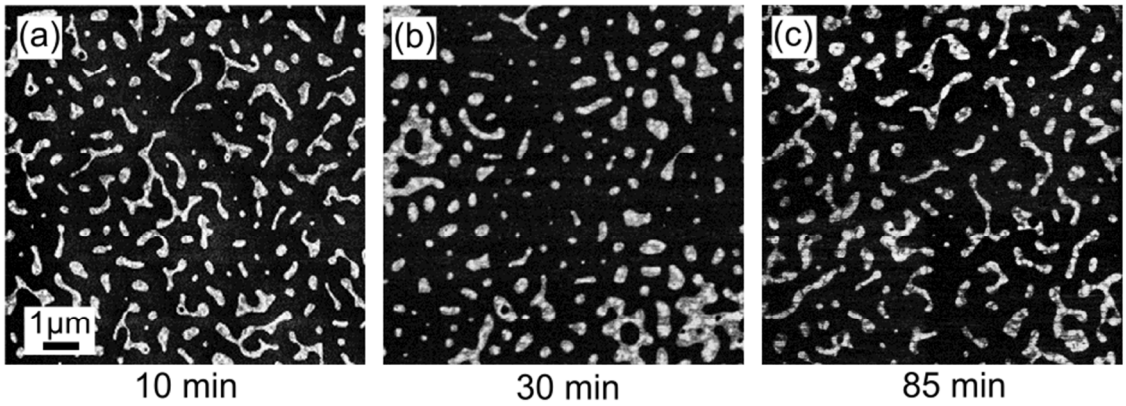

Figure S22: AFM phase images of 57:43 PS_2/$PMMA_3$ blends with 20 vol% of RCBB additive. (a) 10 min; (b) 30 min; and (c) 85 min.

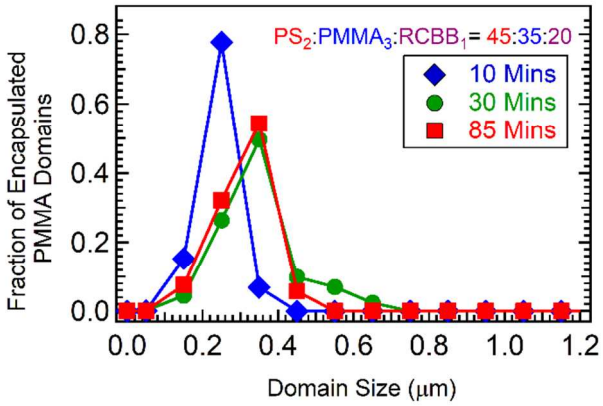

Figure S23: Domain size distribution of 57:43 $PS_2/PMMA_3$ blends with 20 vol% RCBB additive.

Figure S24 reports the optical microscopy images for PS_2:$PMMA_3$ blends vol ratios 57:43, 52:48 and 43:57 with 20 vol% RCBB additive at 85 minutes annealing. These images show that there is some slight thickness variation over a 5μm length scale except for the 57:43 PS_2: $PMMA_3$ blend system.

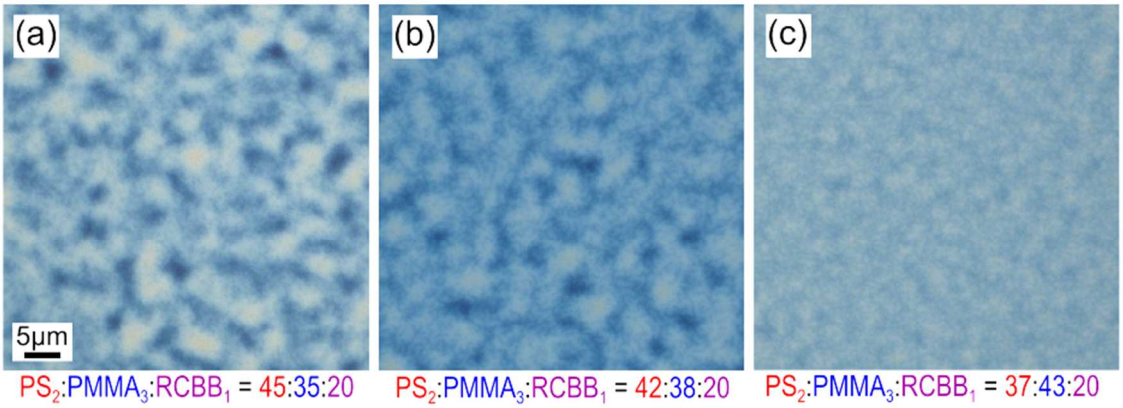

Figure S24: OM images of $PS_2/PMMA_3$ blends with 20 vol% RCBB annealed for 85 minutes. Relative volume of $PS_2/PMMA_3$ blends is fixed at (a) 57:43, (b) 52:48 and (c) 47:53.

Effects of RCBB Backbone Length (Additional Data)

Figure S25 illustrates the effects of RCBB backbone length on the phase morphology of a 57:43 PS_2:$PMMA_3$ blend at a 20 vol% additive concentration. As seen in the main paper, we observe the same three-phase to two-phase transition when the average RCBB backbone length decreases from N_b = 115 (Figure S25a) to N_b = 52 (Figure S25b).

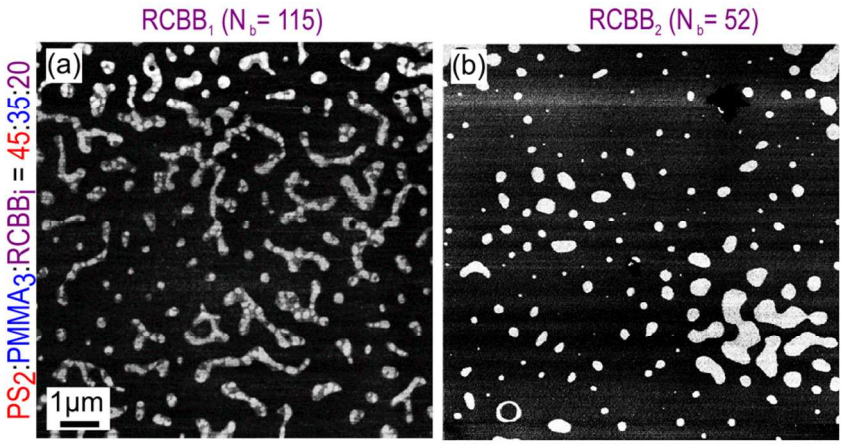

Figure S25: AFM phase images of 57:43 PS_2/$PMMA_3$ blend with 20 vol% of RCBB additives of different backbone lengths and annealed for 85 min. The backbone length of the RCBB additives (a) $RCBB_1$ (N_b=115) and (b) $RCBB_2$ (N_b = 52).

We performed the same test on the low molecular weight PS_1 and $PMMA_2$ homopolymers at volume ratios of 57:43, 52:48, and 43:57. The results of this test is reported in Figure S26. For this system, we do not observe any phase transition with decreasing RCBB backbone length. This behavior is expected since the $RCBB_1$ with longer backbone length (N_b = 115) is already miscible in the PMMA matrix. Hence, the shorter RCBB additive, i.e., $RCBB_2$ (N_b=52) will also be miscible in the PMMA matrix.

At a fixed blend volume ratio of 57:43 PS_1:$PMMA_2$ with 20 vol% $RCBB_i$ Additive (PS_1/$PMMA_2$/$RCBB_i$ = 45:35:20) (Figure S26a-b), the blend phase separates into a continuous PS-rich matrix with minority PMMA-rich domains for both $RCBB_1$ (N_b = 115) and $RCBB_2$ (N_b=52) additives. However, the PS phase in the blend system with $RCBB_2$ (N_b=52) appears more swollen than the PS phase in the $RCBB_1$ blend system. In addition, we observe that the blend system with $RCBB_2$ (N_b=52) yielded smaller PMMA domains compared to the blend system with $RCBB_1$ (N_b=115). Similar observations are also observed at a 52:48 PS_1:$PMMA_2$ blend system with 20 vol% RCBB additive (PS_1/$PMMA_2$/$RCBB_i$ = 42:38:20) (Figures S26c-d).

When the blend volume ratio of PS_1:$PMMA_2$ is fixed at 47:53 with 20 vol% RCBB additive (PS_1/$PMMA_2$/$RCBB_i$ = 37:43:20) (Figures S26e-f), we observe a PMMA-rich matrix with minority PS-rich domains with $RCBB_1$ (N_b = 115) and a co-continuous structure with $RCBB_2$ (N_b=52).

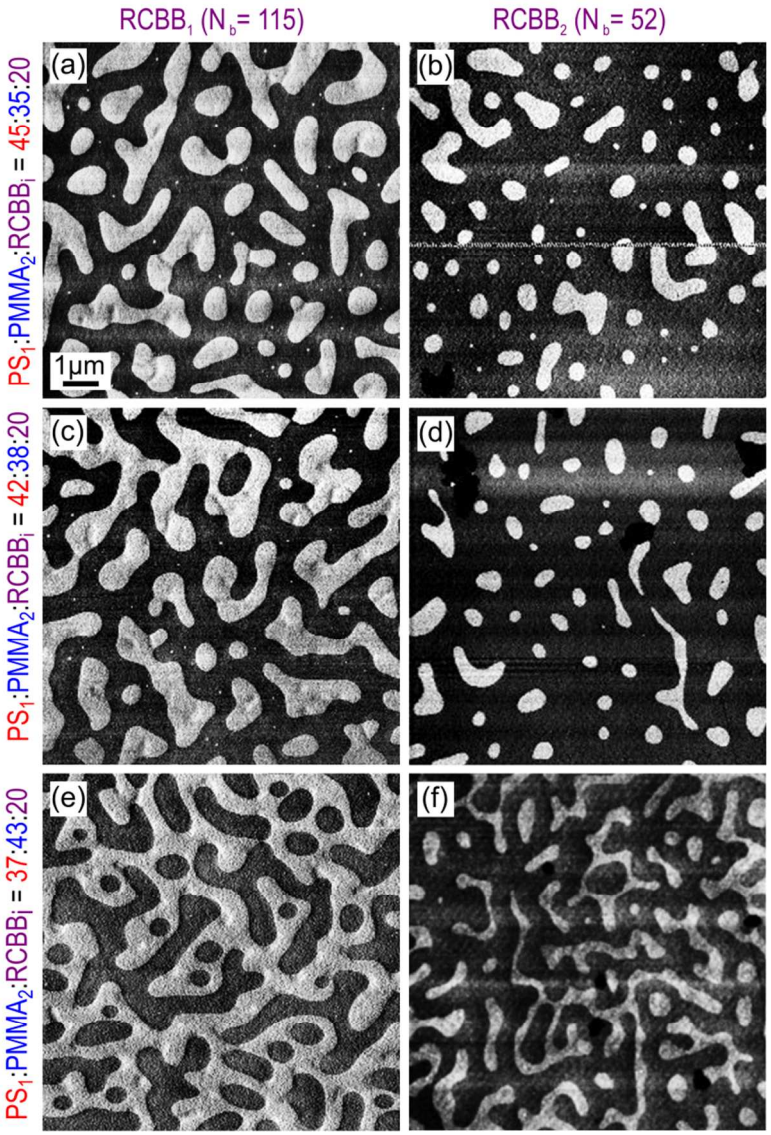

Figure S26: AFM phase images of $PS_1/PMMA_2$ blends with 20 vol% of RCBB additives of different backbone lengths and annealed for 85 min. The proportion of $PS_1/PMMA_2$ in blends are (a-b) 57:43, (c-d) 52:48 and (e-f) 47:53. The backbone length of the RCBB additives is fixed in each column (left: N_b=115, right: N_b = 52).

References

(1) Eitouni, H. B.; Balsara, N. P. Thermodynamics of Polymer Blends. In *Physical Properties of Polymers Handbook*; Mark, J. E., Ed.; Springer New York, 2007; pp 339–356.

(2) Kamath, S. Y.; Dadmun, M. D. The Effect of Copolymer Composition on the Dynamics of Random Copolymers in a Homopolymer Matrix. *J. Chem. Phys.* **2006**, *125* (9), 094902.

(3) Lyatskaya, Y.; Balazs, A. C. Using Copolymer Mixtures To Compatibilize Immiscible Homopolymer Blends. *Macromolecules* **1996**, *29* (23), 7581–7587.

(4) Pesek, S. L.; Lin, Y.-H.; Mah, H. Z.; Kasper, W.; Chen, B.; Rohde, B. J.; Robertson, M. L.; Stein, G. E.; Verduzco, R. Synthesis of Bottlebrush Copolymers Based on Poly(Dimethylsiloxane) for Surface Active Additives. *Polymer* **2016**, *98*, 495–504.

(5) Holland, B. J.; Hay, J. N. The Kinetics and Mechanisms of the Thermal Degradation of Poly(Methyl Methacrylate) Studied by Thermal Analysis-Fourier Transform Infrared Spectroscopy. *Polymer* **2001**, *42* (11), 4825–4835.

(6) Hirata, T.; Kashiwagi, T.; Brown, J. E. Thermal and Oxidative Degradation of Poly(Methyl Methacrylate): Weight Loss. *Macromolecules* **1985**, *18* (7), 1410–1418.

(7) McNeill, I. C.; Razumovskii, L. P.; Gol'dberg, V. M.; Zaikov, G. E. The Thermo-Oxidative Degradation of Polystyrene. *Polym. Degrad. Stab.* **1994**, *45* (1), 47–55.

(8) Wilkie, C. A. TGA/FTIR: An Extremely Useful Technique for Studying Polymer Degradation. *Polym. Degrad. Stab.* **1999**, *66* (3), 301–306.